Adsorption of organic molecules on carbon surfaces: Experimental data and molecular dynamics simulation considering multiple protonation states

Robin Wagner [a,‡], Saientan Bag [b,‡], Tatjana Trunzer [c,‡], Paula Fraga-García [c], Wolfgang Wenzel [b], Sonja Berensmeier [c], Matthias Franzreb [a,*]

[a] Institute of Functional Interfaces, Karlsruhe Institute of Technology, Hermann-von-Helmholtz-Platz 1, 76344 Eggenstein-Leopoldshafen, Germany
[b] Institute of Nanotechnology (INT), Karlsruhe Institute of Technology (KIT), Karlsruhe, Germany
[c] Bioseparation Engineering Group, Technical University of Munich, Boltzmannstraße 15, 85748 Garching, Germany

HIGHLIGHTS

- Adsorption model of organics with multiple protonation and zwitterionic forms.
- Loadings of maleic acid and phenylalanine over a wide pH and concentration range.
- Prediction of the model parameters using molecular dynamics (MD).
- Model parameters fitted via genetic algorithm compared to MD model parameters.
- Explanation of pH impact on adsorption and vice versa.

GRAPHICAL ABSTRACT

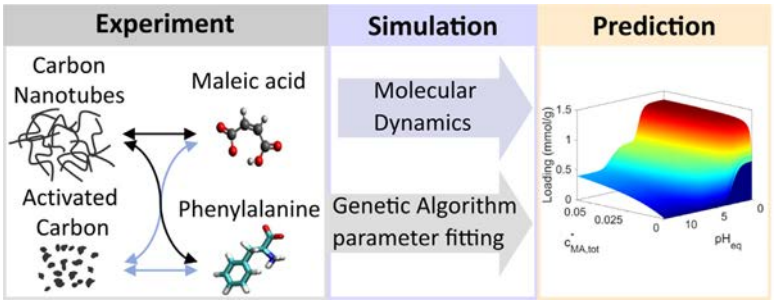

ARTICLE INFO

Keywords:
Organic acids
Molecular dynamics
Genetic algorithm
pH dependence
Activated carbon
Carbon nanotubes
Moreau isotherm

ABSTRACT

Owing to their high specific surface and low production cost, carbon materials are among the most important adsorption materials. Novel usages, for instance in pharmaceutical applications, challenge existing methods because charged and strongly polar substances need to be adsorbed. Here, we systematically investigate the highly complex adsorption equilibria of organic molecules having multiple protonation states as a function of pH. The adsorption behavior depends on intermolecular interactions within the solution (dissociation equilibria) and between adsorbed molecules on the carbon surface (electrostatic forces). For the model substances maleic acid and phenylalanine, we demonstrate that a custom-made genetic algorithm is able to extract up to nine parameters of a multispecies isotherm from experimental data covering a broad pH-range. The parameters, including adsorption affinities, interaction energies, and maximum loadings were also predicted by molecular dynamics simulations. Both approaches obtained a good qualitative and mostly also quantitative description of the adsorption behavior within a pH-range of 2–12. By combining the determined isotherms with mass balances, the final concentrations and pH-shifts of batch adsorption experiments can be predicted. The developed modeling

Abbreviations: AC, Activated carbon; CFX, Ciprofloxacin; CNT, Carbon nanotubes; CNT-K, Multiwalled carbon nanotubes; DFT, Density functional theory; DMD, Discrete molecular dynamics; GA, Genetic algorithm; GAFF, Gernalized Amber force field; IEP, Isoelectric point; MA, Maleic acid; MD, Molecular dynamics; NOM, natural organic matter; Phe, Phenylalanine; PMF, Potential of mean force; QM/MM, Quantum Mechanics/Molecular Mechanics; SD, Standard deviation; SWCNT, Single-walled carbon nanotubes; US, Umbrella sampling; VMD, Visual molecular dynamics; β, Boltzmann factor; $c^*_{MA,tot}$, Concentration in equilibrium; K, Binding affinity; q, Loading; U, Interaction parameter; Wcalc, calculated PMF profile.

* Corresponding author.
E-mail addresses: robin.wagner@kit.edu (R. Wagner), saientan.bag@kit.edu (S. Bag), t.trunzer@tum.de (T. Trunzer), p.fraga@tum.de (P. Fraga-García), wolfgang.wenzel@kit.edu (W. Wenzel), s.berensmeier@tum.de (S. Berensmeier), matthias.franzreb@kit.edu (M. Franzreb).
‡ These authors contributed equally.

Dissociation states
Surface interaction
Aqueous systems

tools can be easily adapted to other types of pH-dependent, multispecies adsorbates and therefore will help to optimize adsorption-based processes in different fields.

1. Introduction

Carbon materials belong to a group of low-cost and widely employed materials. The range of applications extends from energy storage, electronic devices, sensors and catalysts [1–6] to current applications in biology and medicine [7]. Projections of a market size in the range of more than USD 14 billion[1] by 2026 are mainly based on the growing demand for carbon composites in key industries as aerospace and automotive energy and electronics. Furthermore, due to their high surface-to-volume ratio, adsorption processes using carbon-based sorbents are technically widespread and have long been the subject of scientific studies. However, the majority of these applications and studies relate to the adsorption of uncharged organic molecules, such as aliphates, aromates, natural organic matter (NOM), etc. [8]. More recently, however, there has also been an increased interest in the use of these sorbents for charged species, which include biopharmaceuticals, micropollutants, such as pesticides, or heavy metals, all of which may occur in low concentrations. Another very important area of application is the development of novel activated carbon filters in drinking water treatment. Moreover, a growing number of systems and processes use carbon-based sorbents. Some examples are fluidized bed electrode reactors [9,10], capacitive deionization devices and other preparative electrosorption techniques [11–17].

The key emerging challenge to develop scalable processes to selectively filter charged species at low concentration is the complex composition of the adsorbent mixture as a function of pH. Presently there is a scarcity of systematic experimental data for small carbonic acids and other soluble molecules as amino acids and a lack of models that can explain and ideally predict this behavior on the basis of first-principles simulations. To overcome this shortcoming, we present a model that (1) predicts adsorption in systems with complex dissociation behavior, (2) combines a molecular dynamics (MD) model with the calculation of theoretical parameters, (3) we demonstrate the validity of the method by comparing the results with experimental data on pH dependent adsorption of two small molecules with different physico-chemical characteristics (e.g. different polarity and solubility).

There have been several publications concerning the adsorption of charged organic molecules on carbon materials in the past. Already in the early 20th century Bartell and Miller [18] investigated the quality of their carbon material by adsorbing organic dyes and later on stated that a hydrolytic effect caused the pH-shift, which occurred during adsorption of organic acids like maleic acid [19]. In a third publication the adsorption mechanism was studied, taking into consideration the effects of the surface of activated carbon and the structure of the adsorbing species [20]. Leopold et al. investigated the adsorption of herbicides on activated carbon for a wide pH-range [21]. The experimental examination of adsorption processes of charged organic molecules on carbon materials continued in terms of the influence of the substitution of single groups in benzene rings [22], the adsorption kinetics for different carbon products [23], as well as for different solution compositions [24] and temperatures [25,26]. More recent experimental investigations focus on practical applications, e.g. Zhang et al. investigated a method to recover adsorbed fumaric acid from carbon material [27]. However, a large amount of publications show that the adsorption, separation or purification of different molecules is an individual phenomenon of the composition of the molecule species, the surrounding environment and at last, the adsorbate. Until today there is no proper method to predict and describe multicomponent molecule-surface interactions completely.

Parallel to the experimental investigations, there have been ongoing efforts to describe the adsorption of charged substances on carbon materials on a theoretical basis. However, simple Langmuir or Freundlich isotherms are built on experimental results, and are often insufficient to describe the interactions occurring during the adsorption of this type of molecules. A description of the simple Langmuir model and its extensions considering multi species systems and interactions is nicely summarized in a recent review by Swenson and Stadie [28]. Here, a first generalization of the original Langmuir model is made by considering the adsorbate to be a mixture of different molecular species competing for the binding sites, which are assumed to be identical in their properties. This version of the Langmuir model is called the competitive multicomponent Langmuir model. Once the different types of adsorbate species are identified, the experimental results are often fitted to this model with binding affinities of the single species, the ratios of their concentrations and the total number of adsorption sites (maximum loading) as parameters. The model thus can capture the effect of external conditions on the adsorption, which can alter one or more of these parameters. One of such external conditions of interest is the pH-value of the adsorbate solution. Depending on the pKa-value, the adsorbates protonate and deprotonate changing their concentration ratio in the solution at different pH. The adsorbent surface can also chemically change altering the adsorption affinity of the adsorbates. Getzen and Ward fitted their experimental isotherms with this kind of multicomponent Langmuir model for one-fold protonated aromatic organic acids, which were adsorbed on activated carbon and underpinned the, at that time controversial theory, that ionized molecules adsorb on carbon as well as uncharged molecules [29]. Later on, they investigated the pH influence on the adsorption and found the pH to affect surface groups on the carbon material [30]. Jain and Snoeyink modified the competitive Langmuir approach by considering the coexistence of different kinds of binding sites [31]. Husson and King described the adsorption process for twice protonated weak acids and compared a model based on a competitive Langmuir equation with the ideal dilute solution theory [32], which was previously described by Müller et al. [33,34]. Xiao and Pignatello measured the adsorption isotherm of several organic acids and bases on graphite and fitted the isotherm with the multicomponent Langmuir model and also with the Freundlich model [35]. The pH dependence was captured by the protonation and deprotonation of the organic acids and bases. Next to approaches based on Langmuir equations, approaches based on the Polanyi adsorption potential theory were applied for the prediction of the adsorption of organic compounds in different solutes [36]. Afterwards, the Polanyi adsorption potential theory was extended to predict the adsorption of competitive molecules on activated car-

[1] https://www.grandviewresearch.com/industry-analysis/advanced-carbon-materials-market

bon [37]. Thereupon, Rosene and Manes tested the model by examination of the
pH-shift during the adsorption of aromatic substances and a competitive compound [38].

Although the Langmuir models described so far are quite powerful to capture a wide variety of adsorption processes, they fail in case the adsorption is cooperative in nature. The cooperativity in the Langmuir model is introduced by adding interaction between the adsorbates. The adsorption of new molecules is influenced by the interaction with another molecule already adsorbed. In the case of a single adsorbate, the resulting Langmuir model is called the cooperative Langmuir model. This cooperative Langmuir model is further generalized in the case of multiple types of adsorbates participating in many body interactions. This type of multicomponent cooperative adsorption model was first derived by Moreau et al., and therefore it is also known as the Moreau model in literature [39]. Haghseresht et al. measured the adsorption isotherm of various aromatic compounds on activated carbon and fitted the results with the Moreau model [40]. Gritti et al. measured the adsorption isotherms of various alcohols with porous silica and fitted the isotherm with non-cooperative and Moreau model depending on whether the alcohol solution is buffered or not [41]. The model we use in this article is a subclass of the Moreau model where there are two or three different types of adsorbates present and only two body interactions between the adsorbates are considered.

Because of the consideration of interactions between the adsorbates, the Moreau model includes a comparably high number of parameters defining the isotherm. Besides the extraction of these parameters from experiments, there exist numerous simulation attempts to understand and predict adsorption in different systems with the goal of easing the accessibility to these parameters, thus reducing experimental time and costs. In simulation there are mainly two different approaches taken. In the first approach, the adsorption affinity of the molecule is computed using Density functional theory (DFT)/ MD simulation and compared with the adsorption affinity obtained from the experiment. Wang et al. calculated the adsorption energy of 36 pollutant molecules adsorbed to a carbon surface using DFT calculation [3]. The adsorption energy values were fitted to an empirical free energy model to predict the binding free energy of arbitrary pollutants. Zou et al. calculated the adsorption energy of organic pollutants to carbon nanotubes (CNT) using DFT calculation and then calculated the adsorption affinity by Boltzmann weighting the adsorption energy [42]. Geitner et al. performed discrete molecular dynamics (DMD) simulation to calculate free energy for the pesticide nanoparticle interaction and calculated the adsorption affinity the same way as Zou et al. [43]. Comer et al., calculated the potential of mean force (PMF) of adsorption of several mainly hydrophobic small molecules to graphene, and further calculated the adsorption affinity by integrating the PMF curve [44]. Veclani et al. performed PMF calculation to quantify the studied the adsorption of the neutral and zwitterionic forms of ciprofloxacin (CFX) on a single-walled carbon nanotube (SWCNT) [45].

The second simulation approach to study adsorption is multiscale in nature, applying DFT/MD simulation to get the adsorption affinity of a single molecule which is further used in different adsorption models to predict the adsorption behavior of a thermodynamically large numbers of molecules. In our work, we take this approach to study the adsorption of maleic acid and phenylalanine to carbon materials represented by a graphene surface. We perform MD simulation to calculate the energetic parameter of binding which we use in the cooperative Moreau model. The innovative contribution is that we consider a polar substance with complex dissociation behavior and an amphiphilic molecule instead of the usually studied strongly hydrophobic molecules. In a very recent work, a similar multiscale modelling approach involving MD simulation and the non-cooperative Langmuir model was adopted by Angelis et al. to predict the adsorption of surfactants to the alumina [46]. Their work demonstrates the advantages of combining MD simulation with theoretical calculations of thermodynamic nature.

In view of this literature survey, the aim of this work was the development of a systematic workflow allowing the derivation of an isotherm model describing the adsorption of multiple charged and non-charged compounds onto carbon materials. Therefore, we choose the experimental investigation and modelling of the adsorption of organic compounds with multiple protonation steps. Two organic model substances, maleic acid as a representative of molecules with multiple deprotonation steps and phenylalanine as a representative of a zwitterionic molecule, were selected. Their adsorption properties onto two industrially relevant carbon materials, activated carbon (AC) and carbon nanotubes (CNT), were investigated for different concentrations and over a wide pH-range. In parallel, the adsorption process was simulated using a cooperative Langmuir model, i.e. a model that takes the interaction of the adsorbed species into account. The model parameters were determined by means of a genetic algorithm from experimental data on the one hand and by parameter predictions using MD simulations on the other hand. To the best of our knowledge, we are the first ones to combine the cooperative Moreau model with the MD simulation. This enables us overcoming the limitations of the classical Langmuir adsorption model for the description of complex protonation equilibria.

2. Material and methods

2.1. Adsorbents and adsorbates

In this study two different carbon materials were used as adsorbents. Activated carbon powder Carbopal SC11PG was purchased from Donau Carbon (Frankfurt, Germany). For Carbopal SC11PG we measured a specific surface area of 909 m^2/g, an average particle size of 37.6 μm and an average pore size of 1.83 nm. Multi-walled carbon nanotubes (CNT-K) were purchased from Future Carbon GmbH (Beyreuth, Germany). The CNT have an outer diameter between 20 and 40 nm and a specific surface area of 200 m^2/g [11]. As the CNT are to a large extent end-capped (>70%), the adsorption is expected to take place on the outer wall [11]. As adsorbates, the organic substances phenylalanine (Phe) and maleic acid (MA) were used as representatives for the interaction study. They differ in their functional groups, dissociation constants and the resulting charge. However, for both substances there exist three differently protonated states which are present in solution in fractions determined by the respective pKa-values and the adjusted pH. The pKa-values of Phe are 1.83 and 9.13 and the isoelectric point (IEP) is at 5.5. In consequence Phe has one positive charge at acidic conditions, one negative charge at basic conditions and is zwitterionic in a broad pH-range around neutral pH.

The two pKa-values of maleic acid are 1.92 and 6.23. In consequence, maleic acid is neutrally charged in strongly acidic conditions and negatively charged in moderate acidic (one negative charge) as well as neutral and basic conditions (two negative charges).

2.2. Batch adsorption experiments

The batch adsorption experiments for AC and CNT powders were conducted at different institutions in the frame of a common project. Therefore, due to the different morphologies of the materials and the available analytical equipment, the applied batch adsorption methods slightly differ for the two carbon adsorbents

investigated. In both institutions the focus was on investigations including a wide pH- and concentration range to obtain adsorption data for all protonation states of the investigated substances.

2.2.1. Adsorption onto activated carbon

The experiments with AC powders were conducted with a ratio of adsorbate to carbon between 0.75 and 3.75 mmol/g (corresponding to a mass ratio of 87–435 mg/g in case of MA and 124–619 mg/g in case of Phe). The ratio was adjusted by keeping the applied amount of AC always at 20 mg and adding 1.5 mL of solution with varying concentrations between 10 and 50 mmol/L. Before mixing, the pH of the adsorbate solution was adjusted to the desired pH by titration using concentrated HCl (1 M, Titripur® Reag. Ph Eur, Reag. USP) or NaOH (2 M, Titripur®). The solutions used for pH-adjustment, as well as the adsorbates maleic acid (MA, >=99%) and L-α-phenylalanine (Phe, >=98%) were purchased from Merck (Darmstadt, Germany). After mixing the carbon material and 1.5 mL of the prepared solutions in 2 mL Eppendorf cups, the suspensions were incubated for 24 h in a thermomixer (Thermomixer comfort, Eppendorf Hamburg, Germany) while shaking at 1000 rpm at room temperature. Afterwards, the reaction vessels were centrifuged at 8000 rpm for one minute to separate the carbon material from the solution. The supernatant was filtered with a 0.45 μm PTFE syringe filter. Finally, the concentrations of the adsorbate molecules remaining in the supernatant were measured photometrically with an EnSpire Multimode Plate Reader (PerkinElmer, Waltham, USA) at wavelengths of 230 nm (L-α-Phenylalanine) and 254 nm (maleic acid). To ensure the reproducibility, every experiment was conducted as triplicate or at least twice.

2.2.2. Adsorption onto carbon nanotubes

On suggestion of the manufacturer, the CNT powder is purified with 1 M HCl at 80 °C for more than 4 h and neutralized afterwards with DI-water. As CNT powder is electrostatically charged and harmful, the CNT are stored in DI-water suspension and used as slurry or wet pellet for all further experiments. At the beginning of the static binding capacity experiments, particles from the storage solution are centrifuged (4000*g*, 5 min, supernatant discarded) and resuspend in DI-water in a particle to DI-water ratio of 2:3. For the further experiments, 2 mL of the homogeneous particle slurry are pipetted and centrifuged (3200*g*, 5 min), the supernatant is discarded and the CNT pellet is incubated with 2 mL of the adsorbate for 24 h, stirred at 250 rpm, at room temperature. The pH-value of the sample is controlled before incubation and afterwards. The supernatant is filtered with a 0.2 μm syringe filter and analyzed in an Agilent HPLC at 258 nm. The experiments are performed as technical triplicates, each sample is analyzed three times. The adsorbates Maleic acid (MA, >=99%, Sigma Aldrich Chemie GmbH, Taufkirchen, Germany) and L-Phenylalanine (Phe, >=98%, Sigma Aldrich Chemie GmbH, Taufkirchen, Germany) were used with different initial concentrations between 5 and 30 mM. The pH of the adsorbate solution was set between 1.5 and 9.5, adjusted with either hydrochloric acid (Reg. Ph. Eu, 37%, VWR International) or sodium hydroxide (>=99% p.a., ISO, Carl Roth GmbH & Co. KG, Karlsruhe, Germany).

2.3. Calculation of adsorbent loading using an extended Moreau isotherm

The original Moreau isotherm [39] was developed for a binary mixture of adsorbate molecules (A and B) being present in diluted form in solution. The adsorbates can bind to the binding sites (adsorption site) of the adsorbent. Each binding site of the adsorbent can hold a maximum of two adsorbate molecules[2]. Moreau et al. assumed an interaction between two molecules if they are adsorbed to the same binding site, making the adsorption cooperative in nature. In this context 'cooperative' does not mean that the interaction is always attractive; on the contrary if the two molecules carry the same electrical charge their interaction always will be repulsive. The concentrations of the adsorbates A and B in the solution are c_A and c_B and their binding affinity constants to the adsorbent are K_A and K_B respectively. In case two A molecules are bound to the same adsorption site, there is an interaction energy U_{AA} between them. The interaction energy for two B molecules is U_{BB} and in case there is one A and one B molecule adsorbed in the same adsorption site the corresponding interaction energy is U_{AB}. In this case, the ratio between the number of molecules A bound and the maximum number of molecules that can adsorb to the binding sites is given by:

$$\frac{N_A}{N_{max}} = \frac{q_A}{q_{max}} = \frac{2K_Ac_A + 2c_A^2K_A^2e^{-\beta U_{AA}} + 2c_AK_Ac_BK_Be^{-\beta U_{AB}}}{1 + 2c_AK_A + c_A^2K_A^2e^{-\beta U_{AA}} + 2c_BK_B + c_B^2K_B^2e^{-\beta U_{BB}} + 2c_AK_Ac_BK_Be^{-\beta U_{AB}}} \quad (1)$$

The average number of molecules B bound can be expressed analogously. If A and B are two variants (e.g. differing in their charge) of the same compound, the total loading of this compound can be expressed by simply adding the loadings of A and B:

$$\frac{N_A + N_B}{N_{max}} = \frac{q_{ges}}{q_{max}} = \frac{2K_Ac_A + 2c_A^2K_A^2e^{-\beta U_{AA}} + 4c_AK_Ac_BK_Be^{-\beta U_{AB}} + 2K_Bc_B + 2c_B^2K_B^2e^{-\beta U_{BB}}}{1 + 2c_AK_A + c_A^2K_A^2e^{-\beta U_{AA}} + 2c_BK_B + c_B^2K_B^2e^{-\beta U_{BB}} + 2c_AK_Ac_BK_Be^{-\beta U_{AB}}} \quad (2)$$

To describe the adsorption in our systems using the Moreau model described above, we first identify the fact that among the three different protonation states (see Section 2.1) of maleic acid and phenylalanine (A, B and C), only two of them (A and B or B and C) are present at a particular pH in significant concentrations. The assumption is quite justified, because the pka-values of the maleic acid (pka-values: 1.92 and 6.23) and phenylalanine (pka-values: 1.8 and 9.1) are well separated keeping the possibility of A and C being together in the solution negligible. For the equation of the final isotherm describing the total loading of the compounds, maleic acid or phenylalanine over the full pH-range the contribution of a pairing of A and C in a binding site can be neglected. Therefore, the isotherm of the total loading of a compound with two clearly separated pKa-values is given by:

$$\frac{q_{ges}}{q_{max}} = \frac{2K_Ac_A + 2c_A^2K_A^2e^{-\beta U_{AA}} + 4c_AK_Ac_BK_Be^{-\beta U_{AB}} + 2K_Bc_B + 2c_B^2K_B^2e^{-\beta U_{BB}} + 4c_BK_Bc_CK_Ce^{-\beta U_{BC}} + 2K_Cc_C + 2c_C^2K_C^2e^{-\beta U_{CC}}}{1 + 2c_AK_A + c_A^2K_A^2e^{-\beta U_{AA}} + 2c_BK_B + c_B^2K_B^2e^{-\beta U_{BB}} + 2c_CK_C + c_C^2K_C^2e^{-\beta U_{CC}} + 2c_AK_Ac_BK_Be^{-\beta U_{AB}} + 2c_BK_Bc_CK_Ce^{-\beta U_{BC}}} \quad (3)$$

This equation contains eight parameters describing the affinities and interaction energies of the differently charged variants of the compound. A ninth parameter is given by the maximum number of available binding sites per mass of adsorbent. It must be emphasized, that the parameters themselves are constants for a given combination of carbon adsorbent and organic substance (existing as species with different protonation states depending on the pH). The pH is accounted for by calculating the species distribution in solution by means of the known pKa values and the corresponding dissociation equilibria. Knowing the species distribution, the cooperative multicomponent Moreau isotherm can be applied to calculate the total loading of the substance.

[2] Moreau et al. also discussed the resulting equations if each binding site of the adsorbent can hold a maximum of three adsorbate molecules. However, for the sake of simplicity we restrict to the case of binding sites which can hold either none, one, or a maximum of two molecules.

2.4. Determination of isotherm parameters

2.4.1. Genetic algorithm

As described in the above section, the extended Moreau isotherm considering the cooperative adsorption of molecules having three different protonation states includes nine parameters. Although not all parameters are equally significant at different pH-values, the reproducible determination of such a high number of parameters by trial and error is practically impossible. Therefore, a self-developed genetic algorithm (GA) was applied, because of the known capability of this kind of algorithm to simultaneously fit numerous independent parameters to experimental data [47]. General information about GA can be found elsewhere [48]. In this context, equation (3) was fitted to the experimental results. To find a set of optimal fitting parameters, the calculation was initialized with 10 random parameter sets which were used to calculate the total loading of the carbon material for each of the experimental conditions (N_{exp}). In order to evaluate the quality or so-called fitness (F) of these parameter sets, equation (4) was used as objective function which sums up the squared differences of the experimental (q_{exp}) and the calculated loadings (q_{calc}).

$$F = \sum_{i=1}^{N_{exp}} \left(q_{exp,i} - q_{calc,i}\right)^2 \tag{4}$$

By the help of their fitness, the parameter sets can be ranked (a minimal value of F corresponds with the highest fitness) and new parameter sets for the next evaluation step can be generated by pairing the five best parameter sets, while the parameter of a set was inherited to the new parameter set with a probability of 50%. For each inherited parameter, there was a probability of 20% for a mutation which meant it was set to a random number within the defined range of the parameter. An exception was applied to the set which achieved the highest fitness so far. This set was always preserved by copying it to the next evaluation step without any change. In order to find an optimal parameter set, the described procedure was repeated 50,000 times, which took between approx. 20 s and 3 min, depending on the number of experimental data points available.

To make sure the genetic algorithm did not find a local minimum, the genetic algorithm was conducted 100 times and an average value of the 30 best fits was used for further evaluation. Additionally, by calculating the standard deviation (SD) of the calculated parameters, an impression of the variation of the determined parameter sets could be gained.

2.4.2. Molecular dynamics

Compared to the extraction of the parameters of the extended Moreau isotherm of a new substance from experimental data, a direct *insilico* prediction of the parameters would be much less laborious and faster. In the following such an *insilico* approach is introduced, using graphene as a general representative [44,49] of carbon materials. It's worth mentioning that, instead of constructing two separate models for activated carbon and CNT, this approach not only saves the computational cost but also provides the transferability of our model to other carbon materials. To estimate the binding affinities of different molecular species onto the graphene surface, we calculated the free energy of binding using an umbrella sampling (US) simulation technique [50,51]. A graphene sheet of 4.26×4.18 nm^2 was built first using visual molecular dynamics (VMD) software [52] and the atomistic models for the different molecular species were built using AVOGADRO [53]. The force field parameters for the graphene sheet and the molecular species were determined using the software AMBERTOOLS [54] with the Generalized Amber force field (GAFF) [55]. The charge on different atoms of the molecular species was assigned using the QM/MM (Quantum Mechanics/ Molecular Mechanics) method as implemented in AMBERTOOLS. The pH dependent atomic model of the molecules were constructed by considering the different dominant protonation states (with different total charge) of the molecules at different pH (see Scheme 1 and Scheme 2 in our manuscript). The graphene atoms were kept without any charge. A simulation box with the molecule in the middle and two graphene sheets at the bottom was prepared thereafter. The entire system was further solvated in water. TIP3P model parameters [56] were used for all the water molecules in the system. Na^+ and Cl^- counter ions were added to neutralize the full system. The parameters for the interaction between the molecule, water, ions and graphene were taken from AMBER99ILDN force field [57]. It's worth mentioning that, we have used AMBER class of force fields in our simulations, which is one of the most recommended class [58,59] of force fields for biomolecular simulation. Periodic boundary condition was imposed in all three (x, y and z) directions. The x- and y-dimensions of the box were kept equal to the x- and y-dimensions of the graphene surface, and the atoms located at the edge of the graphene were connected through bonds via the periodic boundary condition. The initial system prepared for the MD simulation is shown in Fig. 1a below. For more details on MD simulation and free energy calculation methodologies see Supporting Information.

To quantify the relative binding affinity of the different molecular species with the graphene surface, we calculate the binding affinity constant by integrating the free energy curve [44] weighted by Boltzmann probability as follows:

$$K_{calc} = C\int_0^{cutoff} exp(-\beta W_{calc}(z))dz \tag{5}$$

$$K_{calc}{}' = K_{calc}/C = \int_0^{cutoff} \exp(-\beta W_{calc}(z))dz \tag{6}$$

Here $W_{calc}(z)$ is the calculated PMF profile, which is shown in the Supporting Information (Fig. A2) and $\beta(1/k_BT)$ is the Boltzmann factor. *cutoff* is the distance upto which the molecule is interacting with the graphene surface. Please note that the binding affinity is determined only up to a constant *C*. However, irrespective of this constant, the relative binding affinity can be well characterized by $K_{calc}{}'(K_{calc}/C)$. As a first approximation, we take the value of *C* to be 1 and report the binding affinity values. It is worth mentioning that there is another way of evaluating the binding affinity where instead of integrating the full PMF curve, just the minima of the PMF profile is taken [43,46]. However, evaluation of binding affinity by integrating the PMF profile is physically more meaningful, since the integration explores the full shape of the PMF profile. Nevertheless, we also calculated the binding affinity by considering only the PMF minima, which provided comparable results obtained with our choice of binding affinity extraction as shown in the Supporting Information (Fig A3).

To measure the interaction energy between two equal adsorbate species, we chose the equilibrated geometry of maleic acid as it adsorbed on the graphene and made 2 copies of it as shown in Fig. 1c. One of the adsorbate molecules was kept frozen in that geometry while the other molecule was pulled towards it. The interaction energy between the two molecules was measured in the course of pulling. The method of the calculation is schematically described in Fig. 1(c). The interaction energy between different variants of the adsorbate, which was calculated the same way is shown the Fig A4 in the Supporting Information.

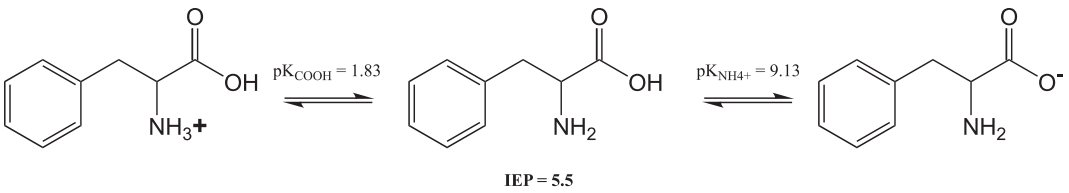

Scheme 1. Charge states of phenylalanine at different pH-values.

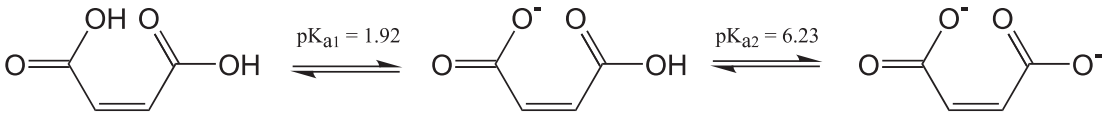

Scheme 2. Charge states of maleic acid at different pH-values.

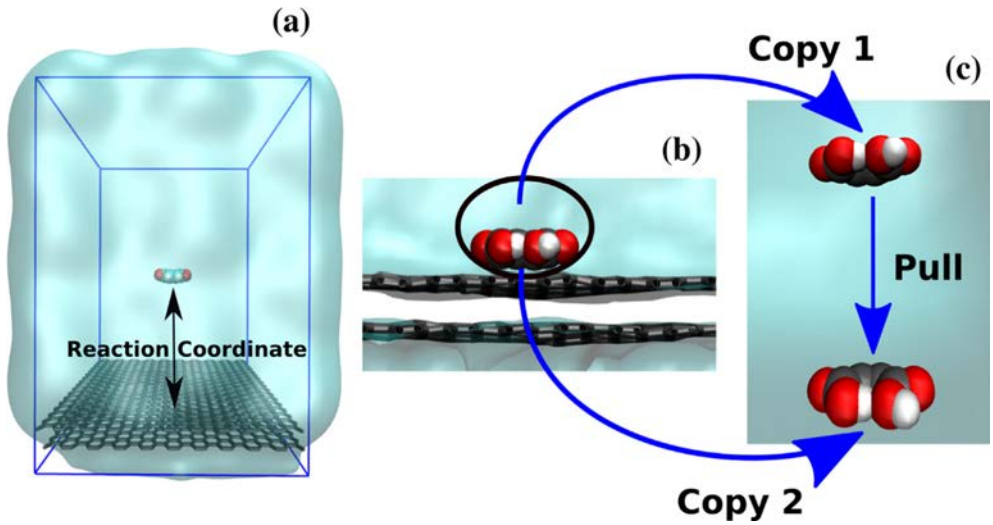

Fig. 1. Molecular Dynamics workflow: (a) A Snapshot of the initial system prepared for molecular dynamics simulation. The two graphene sheets are positioned in one end of the simulation box and maleic acid is kept in the middle. The surrounding water medium is shown in translucent color, but not in full atomistic detail for clarity. The simulation box is shown in blue lines. Reaction coordinate for the free energy calculation is also highlighted. (b) Simulation snapshot when the maleic acid molecule is adsorbed on graphene. (c) Initial snapshot of a system prepared to calculate the interaction energy between two adsorbed maleic acid molecules. One maleic acid molecule was kept frozen to its adsorbed geometry while another molecule is pulled towards it and the interaction energy is measured. (For interpretation of the references to color in this figure legend, the reader is referred to the web version of this article.)

3. Results

3.1. Adsorption of maleic acid onto activated carbon and carbon nanotubes

At the beginning of our experimental series, we studied the adsorption of maleic acid onto AC and CNT in a broad pH-range between approx. 2 < pH < 12. Maleic acid is a typical representative of a two-protonic acid having pKa-values of pKa1 = 1.92 and pKa2 = 6.23. In Fig. 2 the resulting experimental loadings, indicated as colored circles, are plotted versus the equilibrium pH-value. The color of the symbols shows the resulting equilibrium concentrations. In addition, the continuous lines indicate the Moreau isotherms corresponding with different total equilibrium concentrations of the adsorbate in solution. The required isotherm parameters were obtained independently by MD simulations or via the described genetic algorithm (GA). Having two different carbon materials and two ways of parameter determination, this results in four sets of isotherms shown in the plots (a) to (d) of Fig. 2. Fig. 2a and b show the isotherms describing the adsorption of maleic acid onto AC, with a parameter set determined by GA and MD, respectively. Fig. 2c and d show the corresponding isotherms for the adsorption onto CNT, again with the parameter sets determined by GA and MD, respectively.

In our discussion we start with the experimentally determined loadings of maleic acid onto AC (filled circles in Fig. 2a and b). Because the same experimental data set is used, the corresponding filled circles in Fig. 2a and b are identical. The loadings show a clear relationship towards both, the equilibrium pH as well as the equilibrium concentration. The decrease of the loading with increasing pH can be explained by the related change of the dissociation state of maleic acid [27,32]. If a negatively charged maleic acid species is adsorbed onto the carbon surface, the adsorption of further negatively charged species is hampered. In case of species which are twice negatively charged, this effect is even more pronounced. The isotherm sets in Fig. 2a and b show, that this effect is correctly described by both parameter sets, regardless of whether the determination was made by GA or MD. The isotherms display three plateaus and intermediate transition sections which are in accordance to the pKa-values of maleic acid. Below pH ~ 2 a high fraction of uncharged, fully protonated species of maleic acid is present, resulting in maximum loadings of the adsorbent. A second,

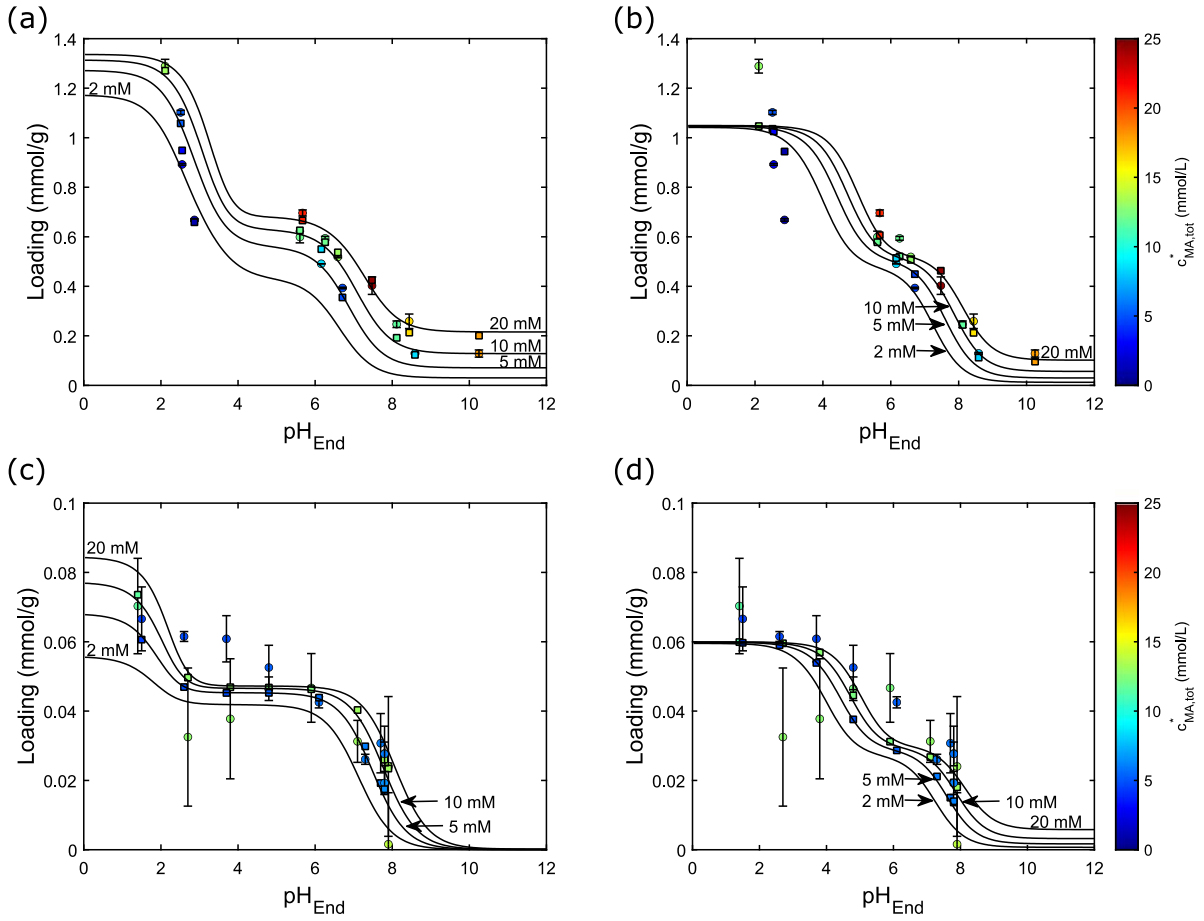

Fig. 2. pH-dependent loading of maleic acid onto AC and CNT: pH dependence of the experimental and predicted loadings of maleic acid onto AC (Fig. 2a; Fig. 2b) and CNT (Fig. 2c; Fig. 2d), respectively. The circles represent experimentally determined loadings and the squares are calculated with the extended Moreau isotherm model for the same conditions. In Fig. 2a and Fig. 2c, the isotherm parameters are extracted from the experimental data by an GA. In Fig. 2b and Fig. 2d, the isotherm parameters are calculated by MD simulations. The continuous lines indicate the Moreau isotherms calculated for the GA or MD parameter sets and constant total equilibrium concentrations of maleic acid of 2, 5, 10, and 20 mM. The experimental standard deviation (SD) is based on experiments conducted as duplicates in case of Carbopal SC11 and as triplicates in case of CNT.

lower plateau can be found for pH-values around 3 < pH < 6, where the main fraction of maleic acid is in a one-fold deprotonated state. And finally, the third plateau can be seen at pH > 8.5 with twice deprotonated maleic acid dominating, resulting in loadings less than one tens of the maximum loadings.

It should be mentioned that for most MD predictions of binding affinities reported in literature are based on free energy calculations of a system where a single molecule approaches the surface of the adsorbent. Therefore, this type of MD simulation cannot capture the interaction effects between multiple adsorbed species. In order to achieve the degree of quantitative agreement shown in Fig. 2b, an extended MD simulation as described in Section 2.4.2 was necessary. When judging the quantitative agreement between the experimental data and the predicted isotherms one encounters the problem that the isotherms are calculated for a fixed total equilibrium concentration of dissolved maleic acid species $c^*_{MA,tot}$. In contrast, in the experiments the $c^*_{MA,tot}$ remaining in solution is varying, depending on the amount of maleic acid adsorbed. Therefore, it cannot be expected that an experimentally determined loading directly hits one of the exemplary isotherms. In order to overcome this problem, we further calculated the theoretical loading corresponding with the equilibrium pH and $c^*_{MA,tot}$ of each experiment and included the results as colored squares in the plots. The corresponding pairs of experimental (circles) and predicted (squares) loadings can be identified by the fact that they share the same pH_{eq} (position on the x-axis) and the same $c^*_{MA,tot}$ (color). From Fig. 2a, it can be seen that the predicted loadings based on parameters fitted via the GA deliver a very good approximation of the experimental loadings over a broad pH-range ($2 < pH_{eq} < 10.5$) as well as a concentration range of $c^*_{MA,tot}$ between 2 and 25 mM. This observation shows that the applied extended Moreau isotherm is basically capable of describing the complex interrelationships of the adsorption of mixtures of charged and non-charged organic species. While this fact might be expected considering the high number of parameters which can be fitted by the GA, the good agreement between the predictions of the isotherm based on parameters determined by MD and the experimental results (see Fig. 2b) is remarkable. The only exception of the good agreement is the pH-range below pH ≈ 4, where the uncharged, fully protonated species of maleic acid starts to form a significant fraction of $c^*_{MA,tot}$. The reason for this discrepancy can be found in Table 1, which summarizes the parameters resulting from GA fitting and MD simulations for the adsorption of maleic acid onto AC and CNT. Comparing the affinity constant of the uncharged species (K_A) calculated by GA and MD it shows that MD postulates a rather high value of around 63,000 while the GA finds only 22,000. Apart from this, the GA predicts a small repulsive interaction between the adsorbed uncharged species, while in the

Table 1
Moreau isotherm parameters of the adsorption of maleic acid onto CNT and AC, determined by GA and MD, respectively. The standard deviation of the GA parameters and the coefficients of determination are based on 30 parameter sets determined with the algorithm.*

	MA on CNT			MA on Carbopal		
Parameter	GA	GA SD	MD	GA	GA SD	MD
K_A (L/mol)	2516	±79	62,856	22,046	±56	62,856
K_B (L/mol)	1728	±25	2391	412	±1	2391
K_C (L/mol)	0.1	±0.0001	6	11.6	±0.009	6
q_{max} (mmol/g)	0.095	±0.0004	0.06	1.37	±0.001	1.05
U_{AA} (kJ/mol)	5	±0.1	0	5.3	±0.004	0
U_{AB} (kJ/mol)	30	±0.1	0	30	±0.02	0
U_{BB} (kJ/mol)	30	±0.01	17	10.7	±0.02	17
U_{BC} (kJ/mol)	30	±0.4	6	30	±0.006	6
U_{CC} (kJ/mol)	30	±0.5	17	30	±0.005	17
R^2	0.68	±0.0004	0.49	0.99	±0.000001	0.89

* The corresponding plots to the determination of R^2 can be found in Fig. A1 for the GA-fits.

MD calculation there is no interaction between uncharged species because the interaction energies are scaled with respect to the neutral–neutral interaction energy (setting the neutral–neutral interaction energy to be zero.) (for more details see Table A3 and Fig. A4 of the Supporting Information). In consequence, all equilibrium concentrations of uncharged maleic acid above approx. 1 mM result in a full saturation of the carbon adsorbent in the calculations based on the MD parameters, independent of the actual concentration value. Fig. 2b shows that this is not the case in the experiments, indicating that the MD overestimates the affinity of uncharged maleic acid towards carbon materials.

Before looking onto the parameters in Table 1 in more detail, the adsorption of maleic acid onto CNT will be discussed (Fig. 2c and d). From the experimental data and the isotherms based on parameters fitted by the GA (Fig. 2c) it can be seen that the pH dependency of the adsorption follows the same trend. Again, uncharged species at low pH show a stronger adsorption affinity than the one-fold charged species around pH 5, and the one-fold charged species show a higher adsorption affinity than the two-fold charged species at pH 8. In absolute numbers, it also shows that the loading capacity of CNT is less than 10% the one of AC. This discrepancy can only be partly explained by the 4.5 times higher specific surface area of the AC. Additional reasons may be differences in the pore size distribution and the tridimensional structure in solution. Moreover, the existence of defects or functional groups on the surface, which depend on the synthesis conditions, may also lead to a different adsorption behavior. Another problem arising from the low loading capacities of CNT is the increased standard deviation of the experimental data, influencing also the quality of the isotherm parameters determined by the GA. Nevertheless, the set of pH-dependent isotherms plotted by the help of the GA parameters in Fig. 2c nicely show the three plateaus and the intermediate transition areas discussed above for the case of the adsorption of maleic acid onto AC. Again, also the isotherms based on the MD parameters are able to describe the experimental data to a satisfying degree.

This is remarkable, because the same set of MD parameters was used, calculated for the interaction of maleic acid with a plain graphene surface. The only exception is the maximum capacity, which cannot be predicted by MD and therefore must be fitted to the experimental results. This fit gives a maximum capacity for the adsorption of maleic acid onto CNT of 0.06 mmol/g, while in the case of AC this value is 1.05 mmol/g. Besides this difference, the calculated isotherms in Fig. 2b and 2d are based on the same set of parameters. Looking at the interaction parameters determined by the GA, a limitation of the Moreau model gets obvious. Despite one exception, all interaction energies U_{xx} involving at least one charged species are set to the maximum of 30 kJ/mol by the GA. This value (30 kJ/mol) represents a strong repulsive interaction and is the maximum of the allowed range for all U_{xx} parameters (X represents A, B and C). If the maximum was set at even higher interaction energies, the GA also selected these values (data not shown), indicating that in these cases the algorithm always approached the maximum repulsive interaction. The reason for this originally unexpected behavior can be found in the circumstance that no matter how large the repulsive interaction U_{xx} is selected, the loading predicted by the Moreau isotherm is reduced to 50% at max, compared to the loading predicted without the repulsive interaction. However, in the experimental data the reduction of the achievable loadings due to repulsive charge interactions seems to be even stronger. Therefore, the GA tries to approach this situation as well as possible by pushing the repulsive interaction parameters to their limits. This is a general problem of Langmuir isotherm variants restricting the interaction of adsorbed species to binary pairs. There are other variants considering also the interaction of e.g. triples, however, the respective equations get even more complex and the number of parameters increases. Therefore, we choose the Moreau isotherm despite its limitations.

3.2. Adsorption of phenylalanine onto activated carbon and carbon nanotubes

A second example for the adsorption of an organic substance with multiple protonation states onto carbon materials was investigated by measuring the adsorption of phenylalanine onto AC and CNT at different initial pH and concentration values. As described in the materials section, phenylalanine differs from maleic acid by the fact that its main conformation over a broad pH-range between approx. 2 and 9 is a zwitterionic form having a positive as well as a negative charge. Besides this zwitterionic form a cationic form dominates at pH < 2 and an anionic form at pH > 9. Therefore, the adsorption of phenylalanine at different pH-values is an interesting case, which covers cations, anions, but also species which have a zero net charge but showing negative and positive regions. As in the case of the adsorption of maleic acid, the experimental results were compared with the predictions of the extended Moreau isotherm using parameters of a GA fit and MD, respectively (Fig. 3). In comparison to the adsorption of maleic acid, the adsorption of phenylalanine shows a rather different adsorption behavior in dependency of the pH. Looking at the adsorption onto AC, the first thing which becomes obvious is that the equilibrium pH of the experiments ended up in a rather narrow pH-range between 6.5 < pH < 9, although the initial pH-values of the solution before mixing with the AC were adjusted to values between pH 4 and pH 9.5. In case of initial pH-values below pH 6, the addition of AC resulted in a strong increase of the pH, ending up in the mentioned narrow pH-range. The reasons for this pH shift will be discussed separately in Section 3.3. Because of the limited

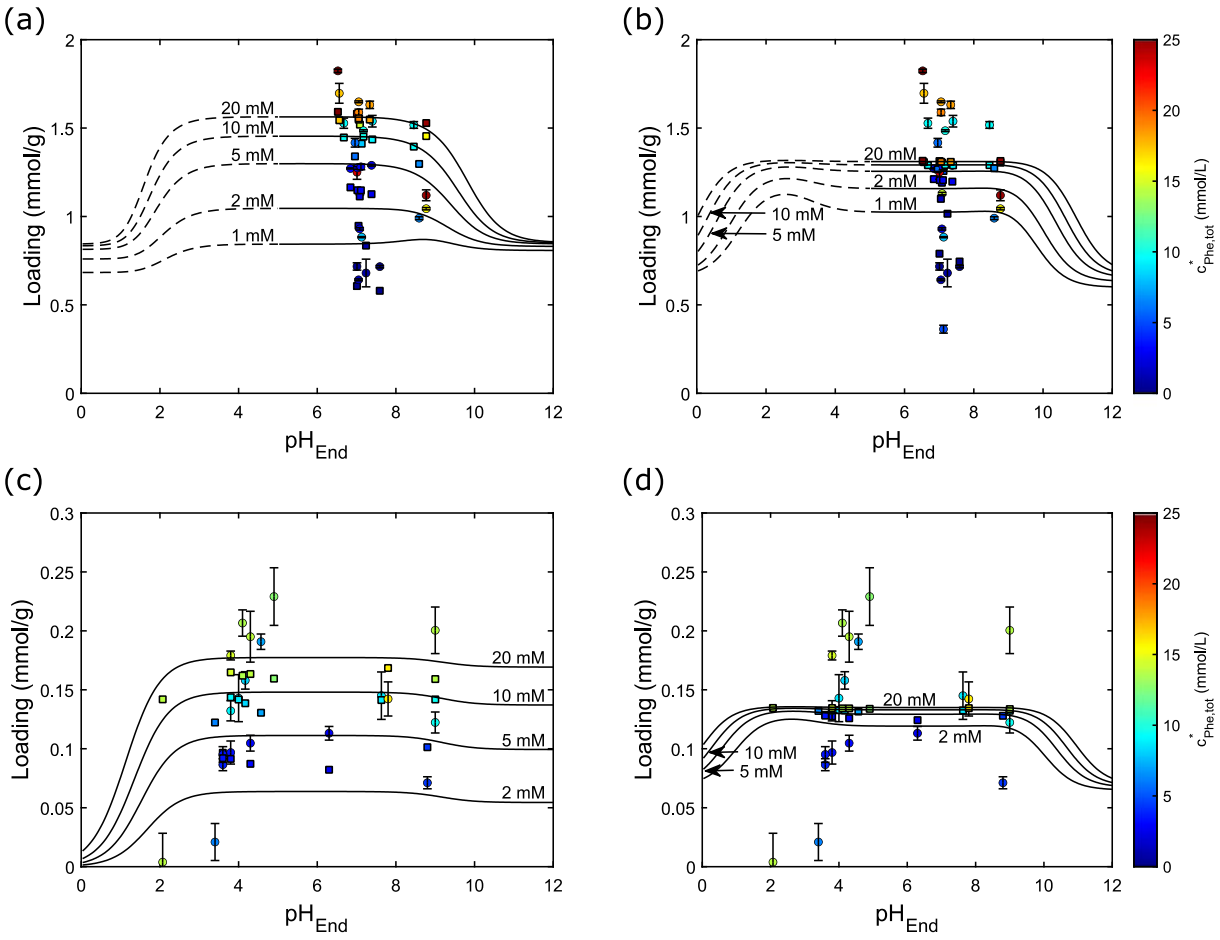

Fig. 3. pH-dependent loading of phenylalanine onto AC and CNT: pH dependence of the experimental and predicted loadings of phenylalanine onto AC (Fig. 3a; Fig. 3b) and CNT (Fig. 3c; Fig. 3d), respectively. The circles represent experimentally determined loading and the squares are calculated with the extended Moreau isotherm model for the same conditions. In Fig. 3a and Fig. 3c, the isotherm parameters are extracted from the experimental data by a GA. In Fig. 3b and Fig. 3d, the isotherm parameters are calculated by MD simulations. The continuous lines indicate the Moreau isotherms calculated for the GA or MD parameter sets and constant total equilibrium concentrations of phenylalanine of 1, 2, 5, 10, and 20 mM. The experimental standard deviation (SD) is based on experiments conducted as duplicates in case of Carbopal SC11 and as triplicates in case of CNT.

equilibrium pH-range, the GA only can deliver meaningful parameters for the affinity constants (K_B, K_C) and the interaction terms (U_{BB}, U_{BC}, U_{CC}), but not for the parameters of species 'A' (cationic phenylalanine), because this species is practically absent above pH 4. While the pH dependency is not fully covered in the experiments, the results show a clear dependence of the equilibrium loading with the equilibrium concentration remaining in solution. This relationship is satisfactorily described by the Moreau isotherms using the parameters determined by the GA (Fig. 3a). Also, the isotherms show a high sensitivity of the loading with respect to the equilibrium concentration in the pH-range between 6 and 8. In the form of dashed lines, Fig. 3a also shows a rough estimation of the course of the loadings at lower equilibrium pH. The estimation of the isotherm parameters defining this course is based on the observed pH-shifts, and will be discussed in Section 3.3.

The calculated adsorption isotherms based on parameters determined by MD show that also in this case the MD derived parameters are able to approximate the general trend of the pH dependency (Fig. 3b). However, as in the case of uncharged maleic acid, the MD calculations overestimate the affinity of the zwitterionic phenylalanine species towards AC. As a result, even low equilibrium concentrations of 2 or 5 mM correspond to almost saturated loadings. In consequence, the fit algorithm for the only unknown parameter q_{max} selects a medium value of around 1.3 mmol/g and the concentration dependence is not sufficiently reflected. In Fig. 3c and 3d the pH dependency of the adsorption of phenylalanine onto CNT is plotted. In case of the experiments with CNT also low equilibrium pH-values could be realized, showing a clear drop of the achieved loading. Again, the zwitterionic form of phenylalanine shows a strong dependence between its adsorption and the equilibrium concentration in solution. While the isotherms based on GA parameters are able to describe these relationships satisfactorily, the MD derived parameters (which are the same than the ones used for the adsorption of phenylalanine onto AC) give the correct trend with respect to pH, but cannot explain the concentration dependency quantitatively, because of the overestimation of the binding affinity. Just like the adsorption behavior of maleic acid, the qualitative dependency of the loading of phenylalanine in relation to the pH can be explained by the charge of the molecules. Phenylalanine is charged positively in its fully protonated conformation and behaves in most respects like a neutral molecule in the one-fold deprotonated, zwitterionic form due to a neutralization of the positive and the negative charge [60]. Therefore, the zwitterionic form shows the strongest tendency to adsorb onto carbon surfaces. In order to describe this trend correctly, the MD calculations have to consider the interaction energies of the charged molecule species. Calculating only the affinity parameter for the adsorption of a single molecule onto a graphene surface, the cationic phenylalanine species shows a remarkably high value (see Table 2), which on its own would pre-

Table 2
Moreau isotherm parameters of the adsorption of phenylalanine onto CNT and AC, determined by GA and MD, respectively. The standard deviation of the GA parameters and the coefficients of determination are based on 30 parameter sets determined with the algorithm.**

	PHE on CNT			PHE on Carbopal		
Parameter	GA	GA SD	MD	GA	GA SD	MD
K_A (L/mol)	0.1	±0.04	56,525	*2000**	±0	56,525
K_B (L/mol)	97	±2	3347	1485	±109	3347
K_C (L/mol)	78	±2	4518	10,593	±697	4518
q_{max} (mmol/g)	0.45	±0.004	0.16	1.71	±0.01	1.33
U_{AA} (kJ/mol)	29	±1	38	*30**	±0	38
U_{AB} (kJ/mol)	30	±0.07	0	*30**	±0	0
U_{BB} (kJ/mol)	30	±0.004	0	2.6	±0.3	0
U_{BC} (kJ/mol)	30	±0.01	0	5	±0.2	0
U_{CC} (kJ/mol)	30	±0.4	19	30	±0.03	19
R^2	0.32	±0.002	−0.09	0.38	±0.002	0.31

* These parameters are estimated by the help of the course of the resulting pH-shift discussed in Section 3.3.
** The corresponding plots to the determination of R^2 can be found in Fig. A1 for the GA-fits.

dict a high adsorption of phenyalanine at low pH-values. However, even this high affinity parameter is overruled by the strong repulsive interaction between adsorbed molecules originating from their charge.

3.3. pH-shifts during the adsorption of maleic acid

In many of our experiments, we observed a pronounced pH-shift occurring during the adsorption of the mixed adsorbates onto the carbon materials. This effect is also often described in literature (see e.g. [38]), however, in most cases without detailed explanations or attempts to model the pH shift quantitatively. The reason for the pH-shift during the adsorption of substances with multiple species having differing protonation states, is mainly the preferred adsorption of one of the dissolved species and the subsequent restoration of the equilibrium between protonated and deprotonated species. In the following, the introduced extended Moreau isotherm is applied to predict the pH-shift by combining the equation of the isotherm with the equations of dissociation equilibria in solution and mass balances. The details of the resulting equation system are listed in the Supporting Information.

The discussion of the accuracy of this set of equations starts with the comparison of the experimental and calculated pH-shifts occurring during batch experiments investigating the adsorption of maleic acid onto AC. As shown in Section 3.1, the extended Moreau isotherm delivers an accurate description of the loadings obtained in these experiments, raising the expectation that also the connected processes in solution should be described correctly. As can be seen in the right part of Fig. 4a, this is perfectly true for the prediction of the total equilibrium concentrations of maleic acid, which is the sum of the concentrations of fully protonated as well as one-fold and two-fold deprotonated maleic acid. For all investigated initial concentrations, the measured equilibrium concentrations (colored circles) fully match the predicted values (colored lines) over the whole pH-range. The left part of Fig. 4a shows the measured and calculated pH-shifts ($pH_{eq} - pH_0$) during the same experiments. Although the data basis is not very dense, the measured pH-shifts clearly show two peaks around $pH_0 = 3$ and $pH_0 = 7$, at which the resulting equilibrium pH-value is increased by more than two pH units compared to the initial pH (see the results of the experiments starting at 20 mM and the added dashed line representing the Makima[3] interpolation of the experimental pH-shifts). This means for example that the equilibrium pH of the batch binding experiment of 20 mM maleic acid onto AC starting at pH 3 reached a final pH-value of 5.6. Keeping in mind the logarithmic nature of the pH, this means that the H^+ concentration dropped around a factor 400 during the experiment. The effect of an enhanced pH-shift towards higher pH-values at or slightly above the pKa-values of maleic acid is within our expectations and will be explained for a system starting at $pH_0 \approx pKa1$ in the following. In the mentioned pH-range, the initial solution contains about equal concentrations of fully protonated and one-fold deprotonated maleic acid. When getting into contact with AC, the adsorption of the fully protonated species is strongly preferred, resulting in a depletion of this species in solution. However, the solution almost instantaneously re-equilibrates the dissociation equilibrium of maleic acid by protonating a small part of the one-fold deprotonated species. This reaction consumes protons and consequently increases the pH. An analog explanation holds for batch experiments starting around $pH_0 \approx pKa2$, where the adsorption of one-fold deprotonated species is preferred against the adsorption of two-fold deprotonated species. In between, around pH 5, the solution contains almost only the one-fold protonated species. The adsorption of such a 'single species' system does not disturb the dissociation equilibria of maleic acid and the resulting pH-shift is comparably small.

As can be seen from Fig. 4a and b, the simulation of batch experiments by means of the Moreau isotherm and parameters derived by GA, but also MD, nicely follows the experimental trend. However, the extend of the pH-shift is reduced, reaching values only slightly above one pH unit. As will be discussed in more detail for the case of batch adsorption experiments of phenylalanine onto AC (see next section), the most likely reason for this discrepancy can be found in functional groups at the AC surface. Furthermore, the surface itself also influences the pH; this is one more reason for the discrepancies between model and experimental values. The protonation or deprotonation of these functional groups results in an additional pH-shift if an aqueous solution is contacted with the AC. Independent of the absolute extend of the pH-shift, the model also reflects the trend that solutions with low maleic acid concentrations experience a higher pH shift. The effect can be led back to the increased pH buffering in presence of a higher maleic acid concentration. For the adsorption of maleic acid onto CNT a similar trend of the experimental pH-shift, which is less pronounced due to the smaller specific surface area, can be observed between $2 < pH_0 < 8$. The pH-shift around pKa1 is less pronounced, resulting in a course of the pH-shift not having two clear peaks but rather a continuous rise with a small dip around pH 5. The same dependencies can also be seen in the calculated pH-shifts, however, with almost no pH-shift predicted in case of $pH_0 \approx pKa1$ and the adsorption parameters determined by GA.

[3] Modified Akima piecewise cubic Hermite interpolation (https://blogs.mathworks.com/cleve/2019/04/29/makima-piecewise-cubic-interpolation/).

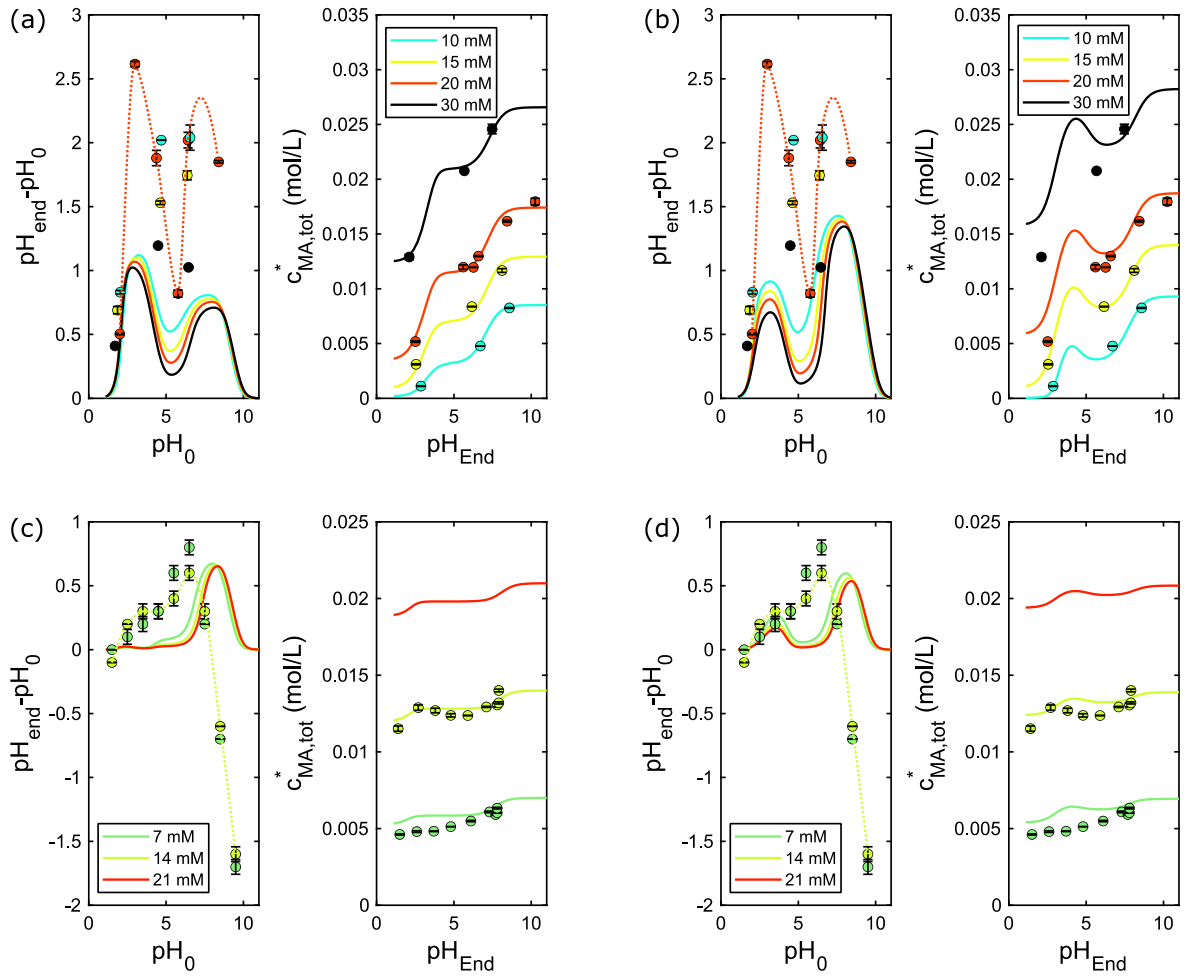

Fig. 4. pH-shift simulation of maleic acid onto AC and CNT: Experimentally observed (symbols) and predicted (continuous lines) pH-shift during the adsorption of maleic acid onto AC (a,b) and CNT (c,d). The prediction of the equilibrium pH and concentration uses the Moreau isotherm based on GA (a,c) and MD (b,d) parameters. The dotted red line shows a Makima-fit for the experimental pH shifts in order to visualize the course of the experimental data. The experimental standard deviation (SD) is based on experiments conducted as duplicates in case of Carbopal SC11 and as triplicates in case of CNT. (For interpretation of the references to color in this figure legend, the reader is referred to the web version of this article.)

3.4. pH-shifts during the adsorption of phenylalanine

Because of its multiple protonation states, it can be expected that also the adsorption of phenylalanine should affect the pH of the solution which gets in contact with the carbon material. From the previous section, we know that both carbon materials show a preferential adsorption of the zwitterionic form of phenylalanine because of its neutral total charge. As a result, the concentration of this species is reduced to a higher degree than the concentrations of the charged species of phenylalanine. At low pH a fraction of the positively charged phenylalanine molecules deprotonates in order to readjust the dissociation equilibria related to pKa1. In consequence, protons are released to the solution and the pH should drop. At pH-values >7 still the zwitterionic form shows preferred adsorption. Therefore, the amine group of negatively charged phenylalanine species captures a proton to readjust the dissociation equilibria related to pKa2 and the pH of the solution rises. Therefore, the pH effects caused by the selective adsorption of different species of phenylalanine should differ from the one observed for the adsorption of maleic acid, where we predicted and measured a rise of the solution pH around pKa1 and pKa2.

When analyzing the pH shift of the respective adsorption experiments with phenylalanine onto AC, at first sight it seems that the results strongly deviate from this prediction. As shown in Fig. A5a of the Supporting Information, the pH shift between the equilibrium pH and the initial pH is strongly positive even at low initial pH-values around 3 or 4. However, the contradiction can be resolved by looking at the pH-shift which is caused by pure AC when suspended in unbuffered solutions of different pH. In Fig. A5b it can be seen that already pure AC causes a strong pH-effect in experiments with the same ratio of carbon to liquid, with a positive pH-shift up to three pH units at a starting pH-value of $pH_0 = 4$. Above $pH_0 = 7$ the pH-shift turns into negative values with a shift of −2.5 units around $pH_0 = 9$. It is known that when dry carbon materials get into contact with water the protonation or deprotonation of functional groups, e.g. carboxyl groups, causes such a pH-shift in the adjacent solution [61]. The higher the specific surface area and the more functional groups are present, the more distinctive is the influence on the pH-value. Therefore, in order to extract the pH-effect caused by the adsorption of phenylalanine, we subtracted the pH-effect caused by contacting AC with pure water from our experimental values (see Fig. 5). After the elimination of the pH-shift caused by surface groups, the remaining pH-shift shows the expected trend moving from a negative pH-shift in the range of pKa1 towards a positive pH-shift in the range of pKa2. The calculation of the pH-shift applying parameters determined by GA also shows this dependency qualitatively (see Fig. 5a). However, the predicted degree of the pH-shift is too small.

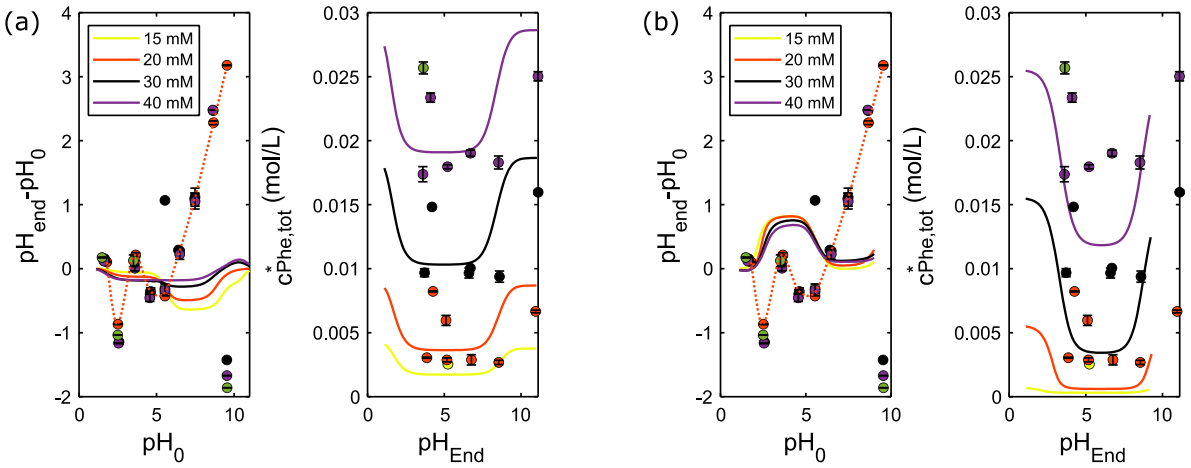

Fig. 5. pH-shift simulation of phenylalanine onto AC: Experimentally observed (symbols) and predicted (continuous lines) pH-shift during the adsorption of phenylalanine onto AC. The experimental pH-shifts were corrected by the pH-shifts caused by AC in deionized water in order to highlight the pH-shift caused by the adsorption of phenylalanine (see Supporting Information). The prediction of the equilibrium pH and concentration uses the Moreau isotherm based on GA (a) and MD (b) parameters. The dotted red line shows a Makima-fit for the experimental pH shifts in order to visualize the course of the experimental data. The experimental standard deviation (SD) is based on experiments conducted as duplicates. (For interpretation of the references to color in this figure legend, the reader is referred to the web version of this article.)

A possible reason might be the high sensitivity of non-buffered solutions in the neutral pH-range around 4–10 towards small inaccuracies in the absolute H^+ concentration. In contrast to the calculated pH shift applying GA parameters, the predicted pH shifts applying MD parameters cannot describe the trend of the pH shift correctly (Fig. 5b). The cause can be found in the very high value of the parameter $K_{A,}$ predicting a preferred adsorption of the positively charged species of phenylalanine, correlating with a positive pH-shift instead of a negative one.

The measured and calculated pH-shifts in case of adsorption experiments of phenylalanine onto CNT are plotted in Fig. A6 in the supporting information. Because of the comparably small adsorption capacities, the calculated pH-shifts are very small, independent if parameters determined by GA or MD are used. In contrast, the measured pH-shifts show a sharp negative peak in the pH-range between approx. 5–7. Again, it is likely that this pH-shift is caused by functional groups at the surface of the CNT. However, despite its extent, the pH-shift in the neutral pH-range does not have a significant influence onto the adsorption behavior. The zwitterionic form is by far the most dominant species of phenylalanine in a pH-range stretching from approx. 3–8. Therefore, the pH-shift does not influence the species of phenylalanine in solution. In consequence, according to our model, there is also no influence on the adsorption behavior. It should be mentioned that the situation would differ if the functional groups causing the pH-shift would significantly contribute in the adsorption process. However, looking at Fig. 3d, it shows that the prediction of almost no pH-dependence of the adsorption of phenylalanine in the mentioned pH-range is confirmed by the experiments.

4. Conclusions

In this study we demonstrated a two-pronged approach for the description and prediction of the adsorption of organic molecules with multiple protonation states onto carbon materials. Both approaches use a cooperative Langmuir model – the extended Moreau isotherm – to calculate the total loading of the organic compound in dependence of the pH and the total equilibrium concentration c^*_{tot} of the compound in solution. Together with the known pKa-values of the compound, the species distribution in the solution is fully defined by pH and c^*_{tot}. The extended Moreau isotherm uses individual affinity constants for the various protonation states and mutual interaction energies of adsorbed species to predict the loading. While the extended Moreau isotherm is used in both approaches, they differ in the way how the named parameters are determined. In the first approach, the parameters are derived by an inhouse-developed genetic algorithm from experimental data. In the second approach, sophisticated molecular dynamics calculations using umbrella sampling are used to calculate the parameters only from the known molecular structures of the compounds and MD force fields. In the case of maleic acid as adsorbate, both approaches were able to achieve a good fit between experimental and calculated loadings in a wide pH-range between 2 and 11. This shows that it is essential to include mutual interactions of adsorbed molecules in case of charged species, however, such interactions commonly have been neglected in most multicomponent adsorption models [62]. In the case of phenylalanine as adsorbate, the quality of the fit between experimental and calculated loadings was less satisfying. However, the main reason for the reduced correlation is given by the stronger scattering of the experimental data and the limited pH-range in which they are available. Nevertheless, the general trend of the dependency of the loading on the pH, and therefore on the species distribution in solution, was captured by both approaches also in this case. Besides the calculation of loadings for given pH and concentration values, we applied the derived isotherms also for the more complex task of predicting the outcome of batch adsorption experiments, something which has not been shown for models considering interactions between the adsorbates before [32,63]. The different affinities of different protonation states of a compound result in a preferred adsorption of one of the dissolved species, corresponding with a disturbance of the dissociation equilibria of the compound in solution. In consequence, the adsorption process is accompanied by chemical reactions in the solution, resulting in a more or less pronounced pH-shift. In combination with mass balances and equations for the description of dissociation equilibria, the derived extended Moreau isotherms were able to explain the observed pH-shifts at least qualitatively. Therefore, this work shows that the derived extended Moreau isotherm allows an improved prediction of the adsorption of substances with multiple protonation states. An important key for the applicability of the isotherm is the description of two systematic procedures enabling to derive the numerous required isotherm

parameters either by a genetic algorithm based on experimental data or via sophisticated molecular dynamics calculations. The same isotherm model and procedures should also be suitable to derive accurate adsorption isotherms and the required parameters for other compounds with multiple charged species, such as charged oxoanions or heavy metal hydroxides. There are many important industrial processes, where such a generalized adsorption model can be used to optimize products and processes, such as the production and purification of carboxylic acids by fermentation of waste biomass and subsequent concentration using activated carbons [64], the adsorptive purification of numerous amino acids [65], or the common removal of arsenate and selenate using charcoals [66].

5. Funding sources

The research was funded by the German Federal Ministry of Education and Research (BMBF) under the project S3kapel [Grant numbers 13XP5038A, 13XP5038B, 13XP5038C]. A part of the experimental data was collected during a stay at the University of Birmingham (UK), funded by the Karlsruhe House of Young Scientists (KHYS).

CRediT authorship contribution statement

Robin Wagner: Conceptualization, Methodology, Software, Investigation, Data curation, Writing - original draft, Visualization. **Saientan Bag:** Conceptualization, Methodology, Software, Data curation, Writing - original draft, Visualization. **Tatjana Trunzer:** Conceptualization, Methodology, Investigation, Writing - original draft, Writing - review & editing. **Paula Fraga-García:** Conceptualization, Writing - review & editing, Supervision. **Wolfgang Wenzel:** Conceptualization, Software, Writing - review & editing, Supervision. **Sonja Berensmeier:** Conceptualization, Writing - review & editing, Supervision, Funding acquisition, Project administration. **Matthias Franzreb:** Conceptualization, Methodology, Software, Data curation, Writing - original draft, Writing - review & editing, Supervision, Project administration.

Declaration of Competing Interest

The authors declare that they have no known competing financial interests or personal relationships that could have appeared to influence the work reported in this paper.

Acknowledgements

We further thank Duy Hung Wolfgang Nguyen Ngoc and Marc-Pascal Apollinaire Tschuschner for their contribution to the experimental studies and interpretation.

References

[1] J. Ignacio, D. Orso, Advanced Carbon Materials Market Size, Share & Trends Analysis Report By Product (Carbon Fibers, Carbon Nanotubes), By Application (Aerospace & Defense, Energy, Automotive), By Region, And Segment Forecasts, 2016–2024, (2016). https://doi.org/GVR-1-68038-160-3.

[2] K.S. Novoselov, V.I. Fal'ko, L. Colombo, P.R. Gellert, M.G. Schwab, K. Kim, A roadmap for graphene, Nature 490 (2012) 192–200, https://doi.org/10.1038/nature11458.

[3] Y. Wang, J. Chen, X. Wei, A.J. Hernandez Maldonado, Z. Chen, Unveiling adsorption mechanisms of organic pollutants onto carbon nanomaterials by density functional theory computations and linear free energy relationship modeling, Environ. Sci. Technol. 51 (2017) 11820–11828, https://doi.org/10.1021/acs.est.7b02707.

[4] M.F.L. De Volder, S.H. Tawfick, R.H. Baughman, A.J. Hart, Carbon nanotubes: present and future commercial applications, Science (80-.) 339 (2013) 535 LP–539, https://doi.org/10.1126/science.1222453.

[5] M. Notarianni, J. Liu, K. Vernon, N. Motta, Synthesis and applications of carbon nanomaterials for energy generation and storage, Beilstein J. Nanotechnol. 7 (2016) 149–196.

[6] E. Pomerantseva, F. Bonaccorso, X. Feng, Y. Cui, Y. Gogotsi, Energy storage: the future enabled by nanomaterials, Science (80-.) 366 (2019) eaan8285, https://doi.org/10.1126/science.aan8285.

[7] N. Panwar, A.M. Soehartono, K.K. Chan, S. Zeng, G. Xu, J. Qu, P. Coquet, K.-T. Yong, X. Chen, Nanocarbons for biology and medicine: sensing, imaging, and drug delivery, Chem. Rev. 119 (2019) 9559–9656, https://doi.org/10.1021/acs.chemrev.9b00099.

[8] G. Newcombe, Chapter Twentysix - adsorption from aqueous solutions: water purification, in: E.J. Bottani, J.B.T.-A., C. M.D. Tascón (Eds.), Elsevier, Amsterdam, 2008, pp. 679–709. https://doi.org/10.1016/B978-008044464-2.50030-4.

[9] A. Tschöpe, S. Heikenwälder, M. Schneider, K. Mandel, M. Franzreb, Electrical conductivity of magnetically stabilized fluidized-bed electrodes – Chronoamperometric and impedance studies, Chem. Eng. J. 396 (2020) 125326, https://doi.org/10.1016/j.cej.2020.125326.

[10] A. Tschöpe, M. Wyrwoll, M. Schneider, K. Mandel, M. Franzreb, A magnetically induced fluidized-bed reactor for intensification of electrochemical reactions, Chem. Eng. J. 385 (2020) 123845, https://doi.org/10.1016/j.cej.2019.123845.

[11] T. Trunzer, T. Stummvoll, M. Porzenheim, P. Fraga García, S. Berensmeier, A carbon nanotube packed bed electrode for small molecule electrosorption: an electrochemical and chromatographic approach for process description, Appl. Sci. 10 (2020) 1133, https://doi.org/10.3390/app10031133.

[12] M. Brammen, P. Fraga-García, S. Berensmeier, Carbon nanotubes-A resin for electrochemically modulated liquid chromatography, J. Sep. Sci. 40 (2017) 1176–1183, https://doi.org/10.1002/jssc.201601102.

[13] F. Kocak, K. Vuorilehto, J. Schrader, D. Sell, Potential-controlled chromatography for the separation of amino acids and peptides, J. Appl. Electrochem. 35 (2005) 1231–1237.

[14] M.W. Knizia, K. Vuorilehto, J. Schrader, D. Sell, Potential-controlled chromatography of short-chain carboxylic acids, Electroanalysis. 15 (2003) 49–54, https://doi.org/10.1002/elan.200390004.

[15] E. Hack, D. Hümmer, M. Franzreb, Concentration of crotonic acid using capacitive deionization technology, Sep. Purif. Technol. 209 (2019) 658–665, https://doi.org/10.1016/j.seppur.2018.08.049.

[16] M. Lenz, R. Wagner, E. Hack, M. Franzreb, Object-oriented modeling of a capacitive deionization process, Front. Chem. Eng. 2 (2020) 3.

[17] M.A. Luciano, H. Ribeiro, G.E. Bruch, G.G. Silva, Efficiency of capacitive deionization using carbon materials based electrodes for water desalination, J. Electroanal. Chem. 859 (2020) 113840, https://doi.org/10.1016/j.jelechem.2020.113840.

[18] F.E. Bartell, E.J. Miller, Adsorption by activated sugar charcoal. I1, J. Am. Chem. Soc. 44 (1922) 1866–1880, https://doi.org/10.1021/ja01430a004.

[19] F.E. Bartell, E.J. Miller, Adsorption by activated sugar charcoal. II1,2, J. Am. Chem. Soc. 45 (1923) 1106–1115, https://doi.org/10.1021/ja01658a003.

[20] F.E. Bartell, E.J. Miller, Adsorption by activated sugar charcoal. III. The mechanics of adsorption, J. Phys. Chem. 28 (1924) 992–1000, https://doi.org/10.1021/j150243a008.

[21] A.C. Leopold, P. van Schaik, M. Neal, Molecular structure and herbicide adsorption, Weeds 8 (1960) 48–54, https://doi.org/10.2307/4040506.

[22] S. Parkash, Adsorption of weak and non-electrolytes by activated carbon, Carbon N. Y. 12 (1974) 37–43, https://doi.org/10.1016/0008-6223(74)90038-4.

[23] M. Baudu, P. Le Cloirec, G. Martin, Pollutant adsorption onto activated carbon membranes, Water Sci. Technol. 23 (1991) 1659–1666, https://doi.org/10.2166/wst.1991.0620.

[24] E. Ayranci, O. Duman, Adsorption of aromatic organic acids onto high area activated carbon cloth in relation to wastewater purification, J. Hazard. Mater. (2006), https://doi.org/10.1016/j.jhazmat.2005.12.029.

[25] M. Otero, C.A. Grande, A.E. Rodrigues, Adsorption of salicylic acid onto polymeric adsorbents and activated charcoal, React. Funct. Polym. 60 (2004) 203–213, https://doi.org/10.1016/j.reactfunctpolym.2004.02.024.

[26] Y.S. Al-Degs, M.I. El-Barghouthi, A.H. El-Sheikh, G.M. Walker, Effect of solution pH, ionic strength, and temperature on adsorption behavior of reactive dyes on activated carbon, Dye. Pigment. 77 (2008) 16–23, https://doi.org/10.1016/j.dyepig.2007.03.001.

[27] K. Zhang, L. Zhang, S.T. Yang, Fumaric acid recovery and purification from fermentation broth by activated carbon adsorption followed with desorption by acetone, Ind. Eng. Chem. Res. 53 (2014) 12802–12808, https://doi.org/10.1021/ie501559f.

[28] H. Swenson, N. Stadie, Langmuir's theory of adsorption: a centennial review, Langmuir 35 (2019), https://doi.org/10.1021/acs.langmuir.9b00154.

[29] F.W. Getzen, T.M. Ward, A model for the adsorption of weak electrolytes on solids as a function of pH: I. Carboxylic acid-charcoal systems, J. Colloid Interface Sci. 31 (1969) 441–453.

[30] T.M. Ward, F.M. Getzen, Influence of pH on the adsorption of aromatic acids on activated carbon, Environ. Sci. Technol. 4 (1970) 64–67, https://doi.org/10.1021/es60036a006.

[31] J.S. Jain, V.L. Snoeyink, Adsorption from bisolute systems on active carbon, J. (Water Pollut. Control Fed. 45 (1973) 2463–2479.
[32] S.M. Husson, C.J. King, Multiple-acid equilibria in adsorption of carboxylic acids from dilute aqueous solution, Ind. Eng. Chem. Res. 38 (1999) 502–511, https://doi.org/10.1021/ie9804430.
[33] G. Müller, C.J. Radke, J.M. Prausnitz, Adsorption of weak organic electrolytes from dilute aqueous solution onto activated carbon. Part I. Single-solute systems, J. Colloid Interface Sci. 103 (1985) 466–483.
[34] G. Müller, C.J. Radke, J.M. Prausnitz, Adsorption of weak organic electrolytes from dilute aqueous solution onto activated carbon. Part II. Multisolute systems, J. Colloid Interface Sci. 103 (1985) 484–492, https://doi.org/10.1016/0021-9797(85)90124-9.
[35] F. Xiao, J.J. Pignatello, Effect of adsorption nonlinearity on the pH–adsorption profile of ionizable organic compounds, Langmuir 30 (2014) 1994–2001, https://doi.org/10.1021/la403859u.
[36] M. Manes, L.J.E. Hofer, Application of the Polanyi adsorption potential theory to adsorption from solution on activated carbon, J. Phys. Chem. 73 (1969) 584–590, https://doi.org/10.1021/j100723a018.
[37] M.R. Rosene, M. Manes, Application of the Polanyi adsorption potential theory to adsorption from solution on activated carbon. VII. Competitive adsorption of solids from water solution, J. Phys. Chem. 80 (1976) 953–959, https://doi.org/10.1021/j100550a007.
[38] M.R. Rosene, M. Manes, Application of the polanyi adsorption potential theory to adsorption from solution on activated carbon. 10. pH effects and "hydrolytic" adsorption in aqueous mixtures of organic acids and their salts, J. Phys. Chem. 81 (1977) 1651–1657, https://doi.org/10.1021/j100532a010.
[39] M. Moreau, P. Valentin, C. Vidal-Madjar, B.C. Lin, G. Guiochon, Adsorption isotherm model for multicomponent adsorbate—adsorbate interactions, J. Colloid Interface Sci. 141 (1991) 127–136, https://doi.org/10.1016/0021-9797(91)90308-U.
[40] F. Haghseresht, S. Nouri, G.Q. Lu, Effects of the solute ionization on the adsorption of aromatic compounds from dilute aqueous solutions by activated carbon, Langmuir 18 (2002) 1574–1579, https://doi.org/10.1021/la010903l.
[41] F. Gritti, G. Guiochon, Influence of a buffered solution on the adsorption isotherm and overloaded band profiles of an ionizable compound, J. Chromatogr. A. 1028 (2004) 197–210, https://doi.org/10.1016/j.chroma.2003.11.106.
[42] M. Zou, J. Zhang, J. Chen, X. Li, Simulating adsorption of organic pollutants on finite (8,0) single-walled carbon nanotubes in water, Environ. Sci. Technol. 46 (2012) 8887–8894, https://doi.org/10.1021/es301370f.
[43] N.K. Geitner, W. Zhao, F. Ding, W. Chen, M.R. Wiesner, Mechanistic insights from discrete molecular dynamics simulations of pesticide-nanoparticle interactions, Environ. Sci. Technol. 51 (2017) 8396–8404, https://doi.org/10.1021/acs.est.7b01674.
[44] J. Comer, R. Chen, H. Poblete, A. Vergara-Jaque, J.E. Riviere, Predicting adsorption affinities of small molecules on carbon nanotubes using molecular dynamics simulation, ACS Nano. 9 (2015) 11761–11774, https://doi.org/10.1021/acsnano.5b03592.
[45] D. Veclani, A. Melchior, Adsorption of ciprofloxacin on carbon nanotubes: insights from molecular dynamics simulations, J. Mol. Liq. 298 (2020) 111977, https://doi.org/10.1016/j.molliq.2019.111977.
[46] P. De Angelis, A. Cardellini, P. Asinari, Exploring the free energy landscape to predict the surfactant adsorption isotherm at the nanoparticle-water interface, ACS Cent. Sci. 5 (2019) 1804–1812, https://doi.org/10.1021/acscentsci.9b00773.
[47] D. Whitley, A genetic algorithm tutorial, Stat. Comput. 4 (1994) 65–85, https://doi.org/10.1007/BF00175354.
[48] M. Srinivas, L.M. Patnaik, Genetic algorithms: a survey, Computer (Long. Beach. Calif). 27 (1994) 17–26. https://doi.org/10.1109/2.294849.
[49] E.R. Azhagiya Singam, Y. Zhang, G. Magnin, I. Miranda-Carvajal, L. Coates, R. Thakkar, H. Poblete, J. Comer, Thermodynamics of adsorption on graphenic surfaces from aqueous solution, J. Chem. Theory Comput. 15 (2019) 1302–1316, https://doi.org/10.1021/acs.jctc.8b00830.
[50] J. Kästner, Umbrella sampling, WIREs Comput. Mol. Sci. 1 (2011) 932–942, https://doi.org/10.1002/wcms.66.
[51] S. Kumar, J.M. Rosenberg, D. Bouzida, R.H. Swendsen, P.A. Kollman, THE weighted histogram analysis method for free-energy calculations on biomolecules. I. The method, J. Comput. Chem. 13 (1992) 1011–1021, https://doi.org/10.1002/jcc.540130812.
[52] W. Humphrey, A. Dalke, K. Schulten, others, VMD: visual molecular dynamics, J. Mol. Graph. 14 (1996) 33–38.
[53] M.D. Hanwell, D.E. Curtis, D.C. Lonie, T. Vandermeersch, E. Zurek, G.R. Hutchison, Avogadro: an advanced semantic chemical editor, visualization, and analysis platform, J. Cheminform. 4 (2012) 17, https://doi.org/10.1186/1758-2946-4-17.
[54] Case, D.A., Belfon, K., Ben-shlom, I.Y., Brozell, S.R., Cerutti, D.S., Cheatham, T.E., AMBER 2020, (2020).
[55] J. Wang, R.M. Wolf, J.W. Caldwell, P.A. Kollman, D.A. Case, Junmei Wang, Romain M. Wolf, James W. Caldwell, Peter A. Kollman, David A. Case, 'Development and testing of a general amber force field' Journal of Computational Chemistry(2004) 25(9) 1157–1174, J. Comput. Chem. 26 (2005) 114. https://doi.org/10.1002/jcc.20145.
[56] W.L. Jorgensen, J. Chandrasekhar, J.D. Madura, R.W. Impey, M.L. Klein, Comparison of simple potential functions for simulating liquid water, J. Chem. Phys. 79 (1983) 926–935, https://doi.org/10.1063/1.445869.
[57] K. Lindorff-Larsen, S. Piana, K. Palmo, P. Maragakis, J.L. Klepeis, R.O. Dror, D.E. Shaw, Improved side-chain torsion potentials for the Amber ff99SB protein force field, Proteins Struct. Funct. Bioinforma. 78 (2010) 1950–1958, https://doi.org/10.1002/prot.22711.
[58] O. Guvench, A. MacKerell, Comparison of protein force fields for molecular dynamics simulations, Methods Mol. Biol. 443 (2008) 63–88, https://doi.org/10.1007/978-1-59745-177-2_4.
[59] A.M. Fluitt, J.J. de Pablo, An analysis of biomolecular force fields for simulations of polyglutamine in solution, Biophys. J. 109 (2015) 1009–1018, https://doi.org/10.1016/j.bpj.2015.07.018.
[60] H. Bannwarth, B.P. Kremer, A. Schulz, Aminosäuren, Peptide, Proteine, in: Basiswissen Phys. Chemie Und Biochem. Vom Atom Bis Zur Atmung – Für Biol. Mediziner, Pharm. Und Agrar., Springer Berlin Heidelberg, Berlin, Heidelberg, 2019: pp. 339–360. https://doi.org/10.1007/978-3-662-58250-3_15.
[61] J.A. Menéndez-Díaz, I. Martín-Gullón, Chapter 1 Types of carbon adsorbents and their production, in: T.J.B.T.-I.S., T. Bandosz (Ed.), Act. Carbon Surfaces Environ. Remediat., Elsevier, 2006, pp. 1–47. https://doi.org/10.1016/S1573-4285(06)80010-4.
[62] P. Iovino, S. Canzano, S. Capasso, A. Erto, D. Musmarra, A modeling analysis for the assessment of ibuprofen adsorption mechanism onto activated carbons, Chem. Eng. J. 277 (2015) 360–367, https://doi.org/10.1016/j.cej.2015.04.097.
[63] C.J. Radke, J.M. Prausnitz, Thermodynamics of multi-solute adsorption from dilute liquid solutions, AIChE J. 18 (1972) 761–768, https://doi.org/10.1002/aic.690180417.
[64] E. Suescún-Mathieu, A. Bautista-Carrizosa, R. Sierra, L. Giraldo, J.C. Moreno-Piraján, Carboxylic acid recovery from aqueous solutions by activated carbon produced from sugarcane bagasse, Adsorption 20 (2014) 935–943, https://doi.org/10.1007/s10450-014-9638-4.
[65] J. Deischter, N. Wolter, R. Palkovits, Tailoring activated carbons for efficient downstream processing: selective liquid-phase adsorption of lysine, ChemSusChem. 13 (2020) 3614–3621, https://doi.org/10.1002/cssc.202000885.
[66] M.K. Mondal, R. Garg, A comprehensive review on removal of arsenic using activated carbon prepared from easily available waste materials, Environ. Sci. Pollut. Res. 24 (2017) 13295–13306.